

Research Article

Enhancing undulation of soft robots in granular media: A numerical and experimental study on the effect of anisotropic scales

Longchuan Li ^a, Chaoyue Zhao ^a, Shuqian He ^a, Qikui Qi ^b, Shuai Kang ^{c,*}, Shugen Ma ^d

^a College of Information Science and Technology, Beijing University of Chemical Technology, Beijing 100029, China

^b School of Engineering Mathematics and Technology, University of Bristol, Bristol BS8 1TH, UK

^c College of Mechanical and Electrical Engineering, Beijing University of Chemical Technology, Beijing 100029, China

^d Thrust of Robotics and Autonomous Systems, The Hong Kong University of Science and Technology (Guangzhou), Guangzhou 511453, China

ARTICLE INFO

Article history:

Received 18 February 2024

Revised 8 March 2024

Accepted 22 March 2024

Available online 26 March 2024

Keywords:

Granular media

Anisotropy

Pseudo-rigid-body model

Soft robot

Undulation

ABSTRACT

Generating efficient locomotion in granular media is important, although it is difficult for robots. Inspired by the fact that sand vipers usually have saw-like scales, in this study, we design a soft undulation robot with tangential anisotropic friction to enhance the undulation performance of soft robots in granular media. A mathematical model was derived and numerical simulations were conducted accordingly to investigate the effectiveness of tangential friction anisotropy for undulation gait generation in granular media. In particular, we introduce a pseudo-rigid-body dynamics model consisting of links and joints while simulating the pneumatic actuation method to more closely approximate the response of soft robots. Moreover, a soft snake-like robot was fabricated, and its forward and reverse undulations were compared in two sets of controlled experiments. The consistency between the experimental results and the numerical simulations confirms that tangential anisotropic friction induces a propulsive effect in undulation, thereby increasing the robot's locomotion speed. This discovery provides new insights into the design of undulation robots in granular environments.

© 2024 The Author(s). Published by Elsevier B.V. on behalf of Shandong University. This is an open access article under the CC BY license (<http://creativecommons.org/licenses/by/4.0/>).

1. Introduction

Granular media, which encompasses materials such as sand and gravel, pose significant challenges and unique opportunities in robotics. The fluid-like nature of granular media requires that robotic movement exhibit high robustness. Many researchers aim to enhance the efficiency of robot mobility in environments where traditional locomotion mechanisms are ineffective, focusing on developing robots that can navigate more effectively in these complex terrains [1–3].

The flexible and elongated body of biological snakes confers a significant advantage in undulating through granular environments [4]. Inspired by the undulation of biological snakes, undulation robots [5,6] offer promising solutions for addressing locomotion challenges in granular media. Although many wheeled undulation robots employ wheels to generate the necessary normal force for undulation, effectively enhancing mobility, the addition of wheels limits their operation to stable, flat, and hard terrains [7–12]. On the other hand, researchers have discovered that designing undulation robots with cylindrical bodies allows for commendable mobility in liquids [13]; however, they cannot overcome granular environments [14].

Moving in granular media poses a significant challenge for undulating robots, primarily because of the intricate interplay between friction and movement. Efficient locomotion in such settings necessitates overcoming the fluid-like behavior of the granular media accompanying the robot's motion. Marvi et al. investigated the frictional properties of biological snakes and revealed that snakes can adjust their friction coefficient to adapt to various terrains, thereby enhancing their movement stability [15]. Following this biological insight, Huang et al. designed digging robots with anisotropic scales to study their effect on robot peristaltic movement [16]. Similarly, inspired by worms, Drotman et al. developed a bioinspired soft digging robot for navigating granular media [17]. Das et al. developed a modular earthworm-like robot that utilizes anisotropic friction to move across diverse terrains [18]. Qi et al. developed a 3D soft undulation robot that uses friction on either side of its body for undulating within confined pipelines [19]. Furthermore, by leveraging tangential and normal friction anisotropies, 3D-printed snakeskin was designed for effective undulation in various outdoor environments [20]. Brnayan et al. designed a soft undulation robot exhibiting friction anisotropy to study the effect of gait parameters on complex terrain navigation [21], later enhancing its undulation performance on flat surfaces with an improved kirigami skin [22].

Although these studies significantly enhanced the mobility of undulation robots in granular environments, substantial room for

* Corresponding author.

E-mail address: kangshuai@buct.edu.cn (S. Kang).

improvement remains. It has been observed that sand-specialist snakes with saw-like scales, which potentially lead to tangential anisotropy, generate more natural undulation gait than those without them [23]. This phenomenon reveals the gait selection mechanism of sand-specialist snakes. However, to the best of our knowledge, the study of using a robotic platform [24] to further test its effectiveness has not yet been conducted. Embedding these passive dynamics into undulation robots simplifies their control system [25,26], and potentially improves their locomotion performance [27]. In this study, leveraging the ease of implementing anisotropic friction in soft robotics, we designed a pneumatic bionic soft undulation robot with tangential friction anisotropy through mathematical modeling to investigate its potential to improve undulation speeds on granular media surfaces. By simulating biological snake movements in granular media and employing a pseudo-rigid-body dynamics model [28,29], the effectiveness of tangential friction anisotropy in enhancing the robot's undulation performance was validated through numerical simulations. Additionally, we developed a prototype of a soft undulation robot integrated with specialized scales to enhance its undulation capability in granular environments. By comparing experimental and simulation analyses, this work confirms the importance of tangential friction anisotropy in improving the efficiency of undulation robot movement in granular media and offers new insights and methodologies for designing undulation robots in such environments.

2. Modeling and simulation

This section presents a pseudo-rigid-body dynamics model that emulates an undulating soft robot comprising three segments capable of bidirectional bending, which are actuated by pneumatic actuators. The model consists of links and joints that connect these links.

2.1. Pseudo-rigid-body modeling

As shown in Fig. 1, the robot model comprises nine identical linkages and eight joints. The centroid of each link is located at (x_i, y_i) (where $i = 1, \dots, 9$) in the global x - y coordinate system. The distances from the centroid to the left and right ends of the link are a and b , respectively. In the sequence from head to tail, each set of three consecutive links and two joints represents a segment of a bidirectional bending pneumatic actuator. Three of these actuators are connected in series. Based on the centroid of the tail link (x_1, y_1) , the generalized coordinate vector of the robot system is $\mathbf{q} = [x_1, y_1, \theta_1, \theta_2, \theta_3, \theta_4, \theta_5, \theta_6, \theta_7, \theta_8, \theta_9]$, where θ_i (for $i = 1, \dots, 9$) is the absolute angle of the link with respect to the global x axis, and the absolute angular difference between subsequent links relative to the previous link is ϕ_j (for $j = 1, \dots, 8$).

To replicate the soft, flexible curvature typical of real soft-bodied robots with our linkage bending, we use the modeling methods of various pseudo-rigid-body dynamics models, introducing distinct torsional springs at each joint. To simulate the actuation mechanisms of pneumatic robots, our approach was informed by the linear spring model, from which we designed an actuation technique [30] that not only simplifies the model but also ensures a motion response commensurate with that of actual robots. The robot system is conceptualized as a linkage-only system, with torsional spring forces, friction, and actuating forces treated collectively as external forces. Because the robot operates within a two-dimensional plane, the motion equation for the robot system, which is influenced by external input forces, is formulated in accordance with the Euler-Lagrange equation as follows:

$$\mathbf{M}(\mathbf{q})\ddot{\mathbf{q}} + \mathbf{C}(\mathbf{q}, \dot{\mathbf{q}})\dot{\mathbf{q}} = -\mathbf{J}_w^T \mathbf{F}_w + \mathbf{f} + \mathbf{u} \quad (1)$$

Here, $\mathbf{M}(\mathbf{q})$ refers to the inertia matrix of the robotic system, and $\mathbf{C}(\mathbf{q}, \dot{\mathbf{q}})$ is the combination of centrifugal and Coriolis force components acting on the robot system. Detailed accounts of $\mathbf{M}(\mathbf{q})$ and $\mathbf{C}(\mathbf{q}, \dot{\mathbf{q}})$ for multi-linked undulation robot systems are available in many documents focused on Lagrangian modeling [31]. As mentioned above, the torsional dynamic coupling between two adjacent linkages is approximated by torsional springs, consisting of linear springs and dampers. Let the deformation of the torsional springs be defined as \mathbf{S}_w , the deformation velocity vector is derived from the following equation:

$$\dot{\mathbf{S}}_w = \begin{bmatrix} \dot{\phi}_1 \\ \vdots \\ \dot{\phi}_j \end{bmatrix} = \mathbf{J}_w \dot{\mathbf{q}} \quad (2)$$

Here, with $j \in \{1 \dots 8\}$, representing the number of torsional springs in the eight joints, the Jacobian \mathbf{J}_w is obtained through $\mathbf{J}_w = \frac{\partial \mathbf{S}_w}{\partial \dot{\mathbf{q}}}$. The vector of the torsional spring forces is represented by

$$\mathbf{F}_w = \begin{bmatrix} k_w^1 \phi_1 + \zeta_w^1 \dot{\phi}_1 \\ \vdots \\ k_w^j \phi_j + \zeta_w^j \dot{\phi}_j \end{bmatrix} \quad (3)$$

where k_w^j and ζ_w^j are the stiffness and damping coefficients of the torsional springs, respectively.

We model the frictional forces as a combination of viscous and Coulomb friction models to satisfy the fundamental characteristics of the frictional forces necessary for robotic movement on the surface of granular media. For friction modeling, the rotation matrix is initially defined as the transformation from the local t - n coordinate system of the frictional force for any given link i to the global x - y coordinate system of the robot's motion (see Fig. 1). This rotation matrix \mathbf{R}_i is expressed as follows:

$$\mathbf{R}_i = \begin{bmatrix} \cos \theta_i & -\sin \theta_i \\ \sin \theta_i & \cos \theta_i \end{bmatrix} \quad (4)$$

The global velocity of link i can be obtained from its local velocity through the mapping matrix as shown below:

$$\mathbf{R}_i \begin{bmatrix} v_t^i & v_n^i \end{bmatrix}^T = \begin{bmatrix} v_x^i & v_y^i \end{bmatrix}^T \quad (5)$$

where v_t^i and v_n^i represent the tangential and normal linear velocities of the i th link, respectively. According to [32], The total frictional force acting on link i is defined as the sum of the viscous and Coulomb frictional forces, denoted respectively by

$$\mathbf{f}_i = \mathbf{f}_\mu^i + \mathbf{f}_\eta^i \quad (6)$$

We represent the friction model for each link i by the following expressions:

$$\begin{cases} \mathbf{f}_\mu^i = -m_b g [\mu_t \operatorname{sgn}(v_t^i) & \mu_n \operatorname{sgn}(v_n^i)]^T \\ \mathbf{f}_\eta^i = -[\eta_t v_t^i & \eta_n v_n^i]^T \end{cases} \quad (7)$$

where $i \in \{1 \dots 9\}$, denotes the number of links, m_b represents the mass of the link, g is the acceleration due to gravity, and μ and η respectively denote the Coulomb and viscous friction coefficients. Moreover, the subscripts t and n refer to the tangential and normal directions of the link. Based on this, we define the anisotropic friction characteristics in the tangential direction of link i . The tangential Coulomb friction coefficient μ_t is determined by the following equation:

$$\mu_t = \frac{\operatorname{sign}(v_t^i) + 1}{2} \mu_{tf} + \frac{-\operatorname{sign}(v_t^i) + 1}{2} \mu_{tb} \quad (8)$$

where μ_{tf} and μ_{tb} represent the Coulomb friction coefficients for the robot's forward and backward undulation, respectively.

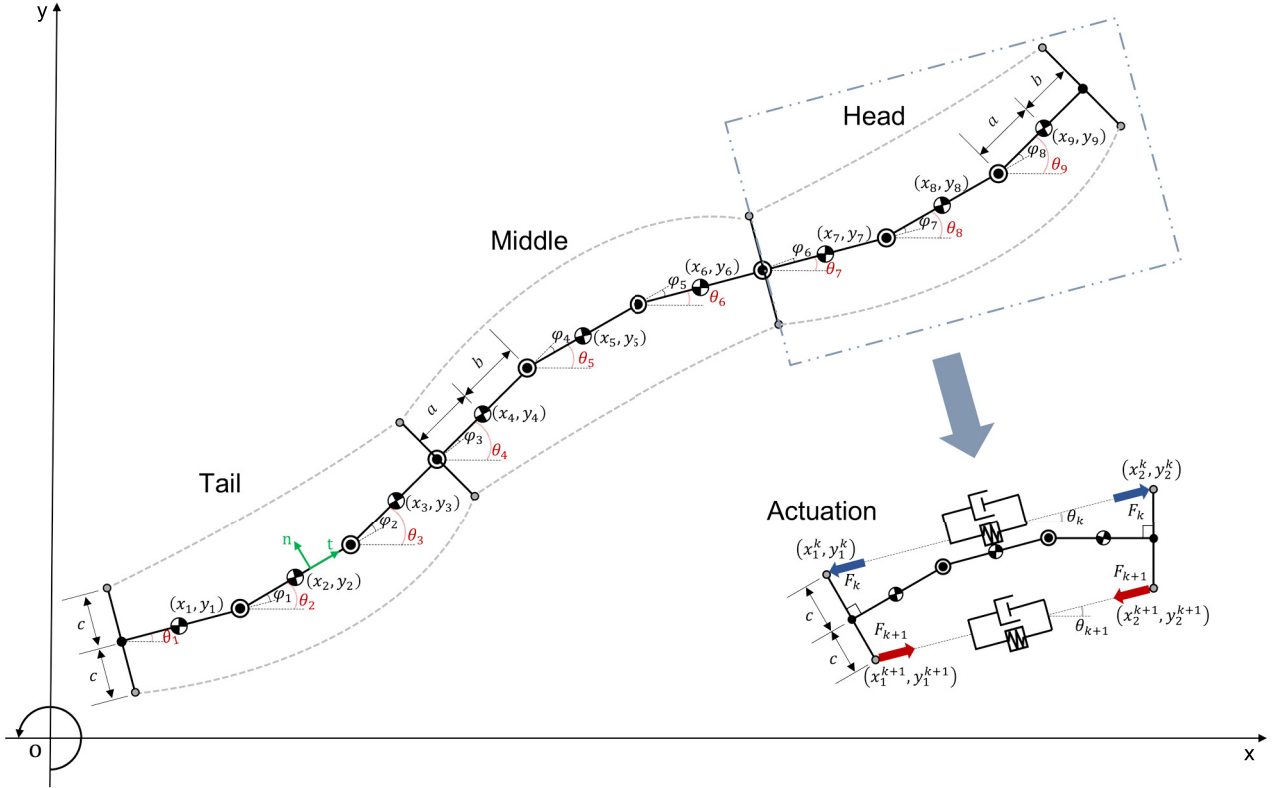


Fig. 1. Pseudo-rigid-body model for a 3-segment undulation robot.

Anisotropic frictional characteristics in the tangential direction can be generated through this asymmetrical design. Subsequently, the frictional force acting on the i th link is mapped to the global x - y coordinate system as

$$\mathbf{f}_{\text{global}}^i = \mathbf{R}_i \mathbf{f}_i \quad (9)$$

Finally, we can express f from Eq. (1) as follows:

$$\mathbf{f} = \sum_{i=1}^9 \mathbf{H}_i^T(\mathbf{q}) \mathbf{f}_{\text{global}}^i \quad (10)$$

where

$$\mathbf{H}_i(\mathbf{q}) = \begin{bmatrix} \frac{\partial v_x^i}{\partial \mathbf{q}} & \frac{\partial v_y^i}{\partial \mathbf{q}} \end{bmatrix}^T \in \mathbb{R}^{2 \times (9+2)} \quad (11)$$

denotes the transpose of the Jacobian matrix of the frictional force for the i th link.

2.2. Pneumatic actuation modeling

Pneumatic actuators achieve left and right bending by alternately inflating the air chambers on both sides. Modeling this actuation method accurately in mathematical form is challenging. We use the linear spring model to simulate the actuation mechanism to approximate the actual response, as shown in the bottom right corner of Fig. 1. At both sides of a segment of the actuator, we employ a linear spring and a damper with a distance of c to it. In this model, the force of the linear spring is independent of the deformation variable and operates periodically. According to the actuation section in Fig. 1, here we show the detailed modeling process of the actuation model. Let the distance between the ends of two tips be defined as \mathbf{D}_k , the relative velocity at the ends of the actuator is given by the following equation:

$$\dot{\mathbf{D}}_k = \begin{bmatrix} \dot{x}_\Delta^k \\ \dot{y}_\Delta^k \end{bmatrix} = \begin{bmatrix} \dot{x}_2^k - \dot{x}_1^k \\ \dot{y}_2^k - \dot{y}_1^k \end{bmatrix} = \mathbf{S}_k \dot{\mathbf{q}} \quad (12)$$

where $k \in \{1 \dots 6\}$, denotes the k^{th} actuation model. Correspondingly, the Jacobian matrix \mathbf{S}_k can be obtained as $\mathbf{S}_k = \frac{\partial \dot{\mathbf{D}}_k}{\partial \dot{\mathbf{q}}} \in \mathbb{R}^{2 \times (9+2)}$. The damping force vector in the k^{th} actuation model is given by $\mathbf{Z}_k = \begin{bmatrix} c_k \dot{x}_\Delta^k \\ c_k \dot{y}_\Delta^k \end{bmatrix}$, where c_k denotes the damping coefficient of the k^{th} damper. The actuation force within the model, which simulates the pneumatic actuator's drive, is characterized by a smoothed periodic square wave as follows:

$$\mathbf{F}_k = \begin{bmatrix} A \cdot \tanh(\epsilon \cdot \sin(\frac{2\pi}{T}t + \psi_k)) \cos \theta_k \\ A \cdot \tanh(\epsilon \cdot \sin(\frac{2\pi}{T}t + \psi_k)) \sin \theta_k \end{bmatrix} \quad (13)$$

where A represents the amplitude of the square wave, ϵ signifies the smoothness of the square wave, T is the period of the square wave, ψ_k denotes the lag phase of the actuation square wave, θ_k is the absolute angle of the k^{th} actuation model with respect to the x -axis. Accordingly, the resultant force vector for the k^{th} actuation model is $\mathbf{F}_k - \mathbf{Z}_k$. Finally, the control input \mathbf{u} in Eq. (1) is formulated as

$$\mathbf{u} = \sum_{k=1}^6 \mathbf{S}_k^T (\mathbf{F}_k - \mathbf{Z}_k) \quad (14)$$

2.3. Simulation analysis

According to the derived dynamics model, we employ MATLAB2023b for conducting numerical simulations to generate a stable undulation gait with periodic actuation forces. We design two sets of controlled experiments to investigate the impact of altering the orientation of the robot's inherent tangential friction anisotropy on its undulatory gait on sand. Details on the parameters and methodologies used in the numerical simulations are below.

We apply two actuation signals in each actuator segment with opposite phases on the left and right sides. Considering the head

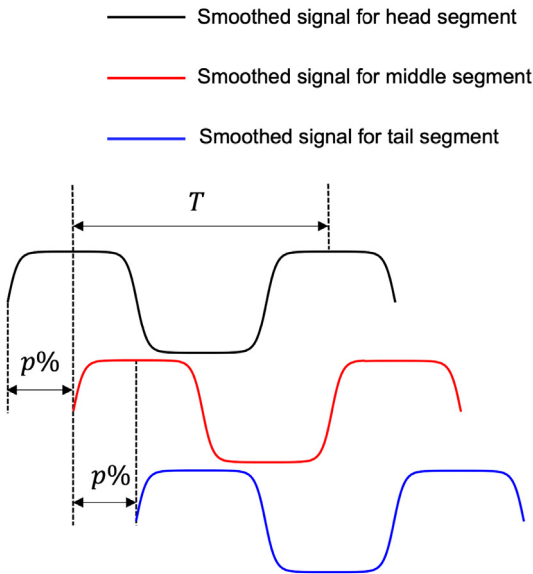


Fig. 2. Diagram of control signals for 3-segment robot model.

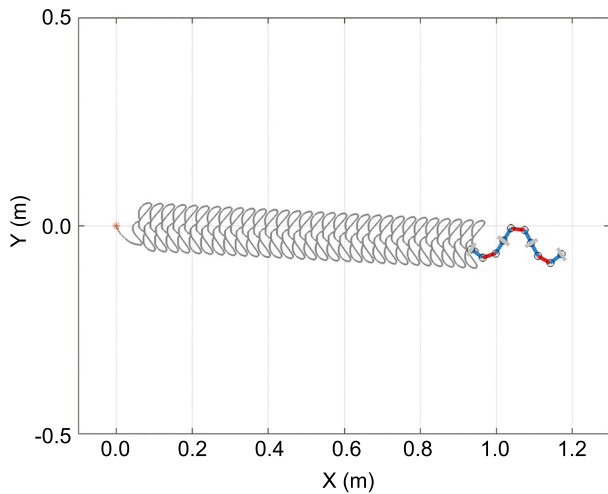


Fig. 3. Simulation of undulation on granular media via pseudo-rigid-body model.

actuator in Fig. 1 as an example, let the phase of the drive on the upper side be defined as ψ_k , then the phase of the drive on the lower side becomes $\psi_k + \pi$. Thus, a single actuator segment alternately swings with the same amplitude on both sides. According to the overall model shown in Fig. 1, the undulation robot is categorized according to its actuators into head, middle, and tail sections. We apply the smoothed square wave signal shown in Fig. 2 to one side of the robot, whereas the phase of the actuation signal on the other side is exactly the opposite. Here, T represents the period of the actuation signal, and $p\%$ denotes the shifting percentage, indicating a phase lag of $p\%$ of T time compared to its previous actuator segment. This phase lag couples the individual swinging of three actuator segments into the robot's undulation gait. Fig. 3 shows a typical gait simulation example, where the detailed parameters used in the simulation are listed in Table 1.

We designed two sets of controlled experiments to investigate the impact of tangential friction anisotropy on the undulation gait on granular media surfaces and to observe its general performance. The experiments involved shifting the robot's friction coefficients, μ_{tf} and μ_{tb} , to alter the orientation of the tangential

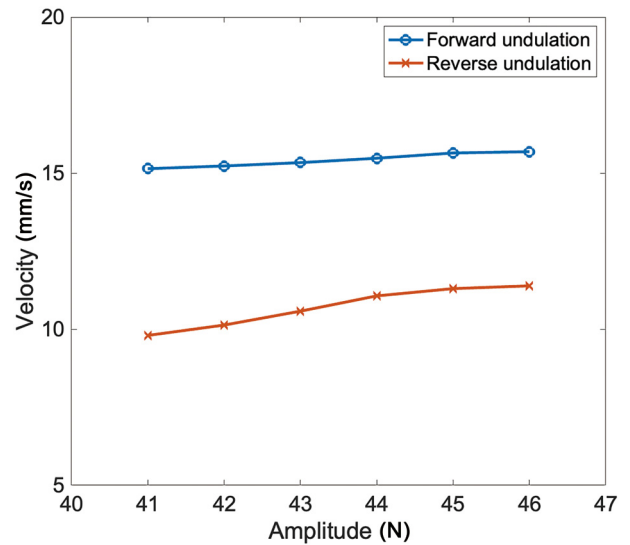


Fig. 4. Comparative results of simulated robot undulation speed.

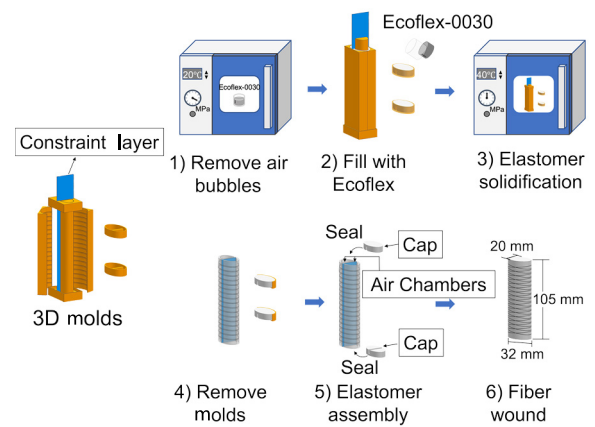


Fig. 5. Fabrication process of fiber-reinforced actuator.

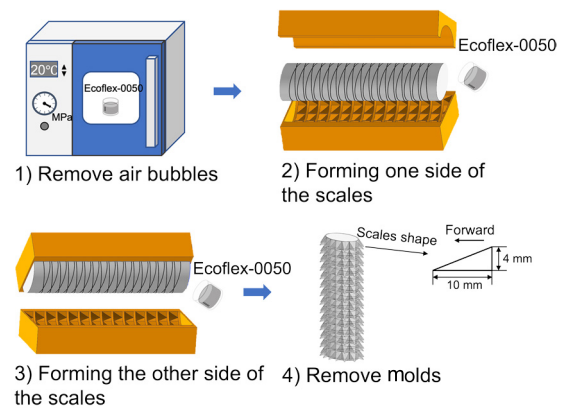


Fig. 6. Fabrication process of the scales.

friction anisotropy. We refer to the undulation under the condition $\mu_{tf} < \mu_{tb}$ as forward undulation, and the undulation under the condition $\mu_{tf} > \mu_{tb}$ as reverse undulation. Both experimental groups were subjected to the same actuation forces as the control

Table 1
Parameters for simulation.

Description	Parameter	Value	Unit
Link mass	m_b	0.02	kg
Length from link mass to left end	a	0.018	m
Length from link mass to right end	b	0.018	m
Robot width	c	0.018	m
Gravitational acceleration	g	9.81	m/s ²
Tangential forward Coulomb friction coefficient	μ_{tf}	0.3	-
Tangential reverse Coulomb friction coefficient	μ_{tb}	0.5	-
Normal Coulomb friction coefficient	μ_n	0.5	-
Tangential viscous friction coefficient	η_t	0.01	-
Normal viscous friction coefficient	η_n	0.05	-
Actuation model damping coefficient	c	[0.1 0.1 0.1 0.1 0.1 0.1]	N-s/m
Joint torsional spring stiffness coefficient	k_w	[0.6 0.8 0 0.6 0.8 0 0.6 0.8]	N/rad
Joint torsional damping coefficient	ζ_w	[0.2 0.2 1000 0.2 0.2 1000 0.2 0.2]	N-s/rad
Actuation period	T	2	s
Shifting percentage	p	33	-
Smoothness of the actuation square wave	ϵ	2	-

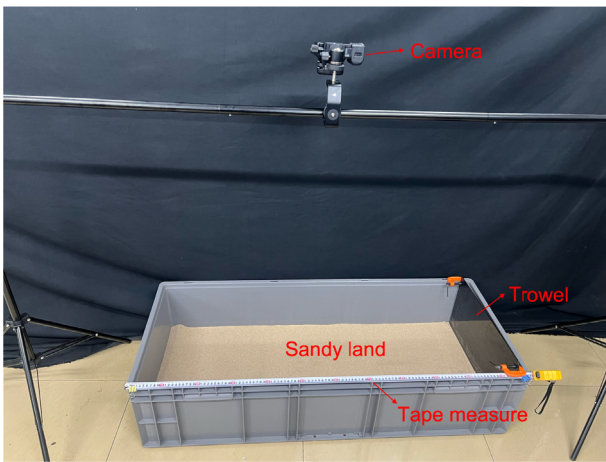


Fig. 7. Experimental environment setup.

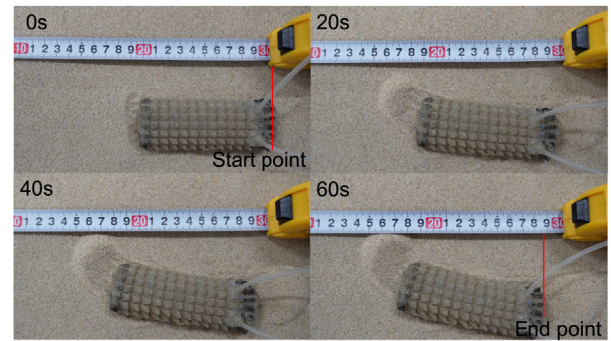


Fig. 9. Verifying tangential anisotropy with peristaltic experiment.

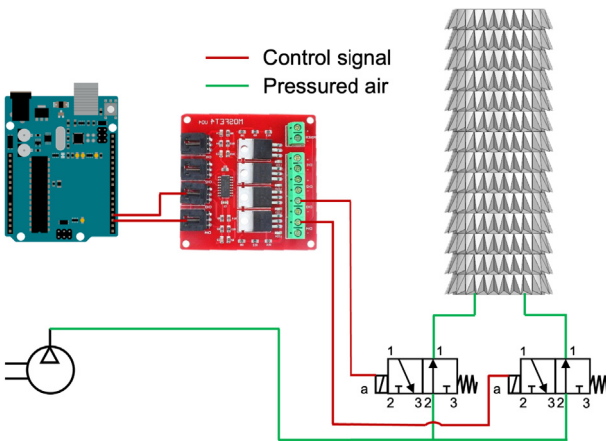


Fig. 8. Peristaltic experiment circuit connection diagram.

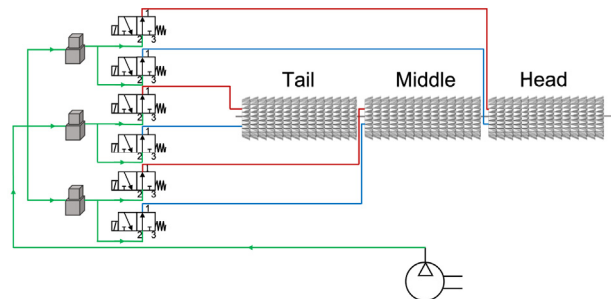


Fig. 10. Undulation experiment pneumatic circuit wiring diagram.

variable. Additionally, to satisfy the frictional properties of the robot's contact with the granular medium, we set one of μ_{tf} or μ_{tb} equal to μ_n .

As illustrated in Fig. 4, the simulation results indicate that both forward and reverse undulation speeds increase as the actuation amplitude increases. However, the forward undulation is consistently faster than the reverse undulation. This indicates

that the tangential friction anisotropy can significantly enhance undulation performance on granular media surfaces.

3. Fabrication and experimental validation

Designing and fabricating a robot platform is necessary for conducting comparative experiments. This section discusses the development of a soft-bodied undulation robot equipped with integrated scales that guarantees the anisotropy of the robot's tangential friction. Experiments were conducted to validate the propulsive effect of this characteristic on the robot's undulation gait on granular media surfaces.

3.1. Platform design and fabrication

The robot's backbone is made of three serially connected, fiber-reinforced actuators. Each actuator has two chambers for



Fig. 11. Illustration of forward and reverse undulation processes driven at 0.55 MPa.

bidirectional bending and an elliptical cross-section to prevent rolling. A layer of non-woven fabric with cloth-like absorbency and paper-like non-extensibility is also embedded between the two chambers. This is aimed at enhancing the actuator's bending amplitude response [33,34]. Fig. 5 shows the fabrication process of the fiber-reinforced actuators. Ecoflex-0030 is poured into the designed and assembled 3D mold after degassing in a vacuum chamber. The mold is removed once the elastomer is formed at a constant temperature of 40 degrees Celsius. The end caps were then coated with Ecoflex-0030 and sealed on both actuator ends. Finally, the solidified elastomer is wrapped with reinforcing fibers in a double helical pattern [35] on the actuator surface. The completed actuator is 10.5 cm long, with an elliptical cross-section where the major axis is 3.2 cm and the minor axis is 2 cm.

To incorporate tangential anisotropic friction into the robot, we examined the findings of Branyan et al. [36], and observed that Kirigami skins could impede the robot's movement in granular media. This impediment arises because the Kirigami skins may allow granular media to become lodged in the gaps between the activated scales during motion, thereby diminishing the anisotropic friction provided by the scales. Finally, the scales were designed with a triangular longitudinal profile [16]. Fig. 6 summarizes the fabrication process of these scales. The direction indicated by the arrows on the scale shapes in the lower right corner of Fig. 6 represents the orientation of the scales adhering to the robot, which is aligned with the direction of the robot's head. The fabricated fiber-reinforced actuator was placed into a 3D scale mold with degassed Ecoflex-0050 covering one-half of the mold. After forming one side of the scales, the scales on the other half were created using the same method without

detaching the elastomer from the mold. The mold was removed when both sides of the scales were formed. The three segments of the actuator with scales were then connected end-to-end using silicone glue, resulting in a pneumatic soft undulation robot with integrated scales.

3.2. Anisotropy verification

We fabricated an actuator without a constraint layer between its two chambers to conduct peristaltic motion experiments and verify whether the scale structure exhibits tangential friction anisotropy. Fig. 7 shows the established experimental environment, in which fine sand from the beach was chosen as the granular medium environment. Before each experiment, the sand was leveled to ensure that the surface was parallel to the ground. During leveling, the thickness of the fine sand was maintained at 9 cm to guarantee that the robot's movement would not come into contact with any other medium. We used a microcontroller board (Arduino, Uno R3) to generate identical pulse signals on two pins for 2 s while alternating high and low output levels to control the opening and closing of two 2-position 3-way solenoid valves. This arrangement, as detailed in Fig. 8, directs compressed air into and out of the two chambers of the actuator, inducing inflation and deflation for actuator elongation and retraction, thus creating a peristaltic gait. As illustrated in Fig. 9, after a 1-min trial, the motion of the actuator demonstrates significant forward displacement on loose sand, confirming the effective tangential friction anisotropy provided by the scale structure.

3.3. Undulation experiment and results

After confirming the effective tangential friction anisotropy of the scale structure, we designed two sets of controlled experiments for the soft-bodied undulation robot: forward and reverse undulations. Fig. 10 provides the detailed connection method for the pneumatic circuit. Here, the blue and red colors of the pneumatic signals within the same actuator indicate that they are out of phase. The experimental period, shifting percentage, and sequence of the actuation signals are the same as those in the simulation. However, due to the inability to alter the robot's tangential friction coefficients from front to back, as in the simulation for reverse undulation, we exchanged the actuation signals of the robot's head and tail to generate reverse undulation conveniently.

The experimental setup is essentially similar to the peristaltic experiments described in the previous section; however, differences include the use of a microcontroller board (Arduino, Uno R3) to generate periodic high and low pulse signals from six output pins, which were connected to six 2-position 3-way solenoid valves to control their operation. Compressed air from the solenoid valves was channeled into the corresponding chambers of the robot. At the air pump's output, three electronic proportional valves (SMC ITV2010-312L) were added to adjust the pressure of the compressed air delivered to each actuator segment. For each set of undulation, we conducted six groups of experiments driven by air pressures of 0.40, 0.45, 0.50, 0.55, 0.60, and 0.65 MPa. Before each experiment, a scraper is used to level the sandy terrain to ensure that it is parallel to the ground. For illustration, two sets of undulations at a driving air pressure of 0.55 MPa, with motion diagrams, are shown in Fig. 11, showcasing the robot's stable undulation after 20 s of motion initiation. Within a minute, the snake moving in a forward undulation traveled an additional 2.5 cm more than in a reverse undulation.

Finally, the undulation velocity is measured and calculated. Three trials were performed for each group, averaging its velocity to reduce uncertainty. As shown in Fig. 12, both forward and reverse undulation velocities positively correlate with the actuation amplitude. In addition, the forward undulation is always faster than the reverse undulation.

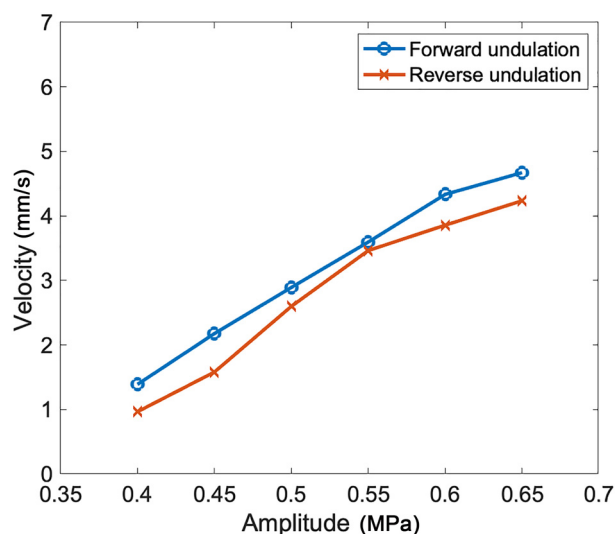


Fig. 12. Comparative results of physical robot undulation speed.

4. Concluding remarks

Through dynamics modeling, numerical simulations, and experimental verification with a physical undulation robot, we demonstrated that tangential friction anisotropy can help create propulsive force in the undulation gait of soft robots on granular media surfaces, thus enhancing their locomotion performance.

Although the tendency and patterns of the simulation and physical experiments are broadly consistent, the experimental results show that observable discrepancies still exist. In the simulations, both forward and reverse undulation speeds increase as the actuation force amplitude increases. However, the increase in forward undulation is much less than the reverse. This differs from the physical robot, where the speed increase for both forward and backward undulation is relatively consistent with the increase in actuation amplitude. We hypothesize that this inconsistency may be due to the more significant nonlinear response in the bending of the physical robot than that in the simulations. Therefore, it is challenging to ensure that the actuator's response in bending increases according to the same pattern, leading to such inconsistencies.

This study focuses on verifying the effect of tangential friction anisotropy on undulation gait performance on granular media surfaces. The inconsistency of the rate increase does not detract from the conclusions drawn from both simulations and physical experiments. Future work will explore the relationships between multiple variables in experiments and the locomotion enhancement brought about by tangential friction anisotropy, further investigating its working mechanisms.

Declaration of competing interest

The authors declare that they have no known competing financial interests or personal relationships that could have appeared to influence the work reported in this paper.

Acknowledgments

This work was supported by Fundamental Research Funds for the Central Universities, China (ZY2301, BH2316, buctrc202215), the National Natural Science Foundation of China (62273340), and the Natural Science Foundation of China Liaoning Province (2021-MS-031).

Appendix A. Supplementary data

Supplementary material related to this article can be found online at <https://doi.org/10.1016/j.birob.2024.100158>.

References

- [1] X. Xiao, R. Murphy, A review on snake robot testbeds in granular and restricted maneuverability spaces, *Robot. Auton. Syst.* 110 (2018) 160–172.
- [2] A. Lopez-Arreguin, S. Montenegro, Towards bio-inspired robots for underground and surface exploration in planetary environments: An overview and novel developments inspired in sand-swimmers, *Heliyon* 6 (6) (2020).
- [3] J. Liu, Y. Tong, J. Liu, Review of snake robots in constrained environments, *Robot. Auton. Syst.* 141 (2021) 103785.
- [4] S. Sharpe, S. Koehler, R. Kuckuk, M. Serrano, P. Vela, J. Mendelson III, D. Goldman, Locomotor benefits of being a slender and slick sand swimmer, *J. Exp. Biol.* 218 (3) (2015) 440–450.
- [5] S. Hirose, *Biologically Inspired Robots*, Oxford Univ. Press, London, U.K., 1993.
- [6] S. Ma, Analysis of creeping locomotion of a snake-like robot, *Adv. Robot., Adv. Robot.* 15 (2) (2001) 205–224.
- [7] X. Ai, H. Yue, W. Wang, Crawling soft robot exploiting wheel-legs and multimodal locomotion for high terrestrial maneuverability, *IEEE Trans. Robot.* 39 (6) (2023) 4230–4239.
- [8] T. Khunnithiwarawat, T. Maneewarn, A study of Active-Wheel snake robot locomotion gaits, in: 2011 IEEE International Conference on Robotics and Biomimetics, ROBOT, 2011, pp. 2805–2809.
- [9] M. Luo, W. Tao, F. Chen, T. Khou, S. Ozel, C. Onal, Design improvements and dynamic characterization on fluidic elastomer actuators for a soft robotic snake, in: 2014 IEEE International Conference on Technologies for Practical Robot Applications, TePRA, 2014, pp. 1–6.
- [10] M. Luo, R. Yan, Z. Wan, Y. Qin, J. Santoso, E. Skorina, C. Onal, Orisnake: design, fabrication, and experimental analysis of a 3-D origami snake robot, *IEEE Robot. Autom. Lett.* 3 (3) (2018) 1993–1999.
- [11] K. Pettersen, Snake robots, *Annu. Rev. Control* 44 (2017) 19–44.
- [12] C. Onal, D. Rus, Autonomous undulatory serpentine locomotion utilizing body dynamics of a fluidic soft robot, *Bioinspiration Biomim.* 8 (2) (2013).
- [13] G. Bianchi, K. Herath, S. Cinquemani, Design of a swimming snake robot, in: *Bioinspiration, Biomimetics, and Bioreplication XII*, 2022, p. 12041.
- [14] R. Maladen, Y. Ding, P. Umbanhowar, D. Goldman, Undulatory swimming in sand: experimental and simulation studies of a robotic sandfish, *Int. J. Robot. Res.* 30 (7) (2011) 793–805.
- [15] H. Marvi, D. Hu, Friction enhancement in concertina locomotion of snakes, *J. R. Soc. Interface* 9 (76) (2012) 3067–3080.
- [16] S. Huang, Y. Tang, H. Bagheri, D. Li, A. Ardente, D. Aukes, H. Marvi, J. Tao, Effects of friction anisotropy on upward burrowing behavior of soft robots in granular materials, *Adv. Intell. Syst.* 2 (6) (2020) 3067–3080.
- [17] D. Drotman, S. Chopra, N. Gravish, M. Tolley, Anisotropic forces for a worm-inspired digging robot, in: 2022 IEEE 5th International Conference on Soft Robotics, RoboSoft, 2022.
- [18] R. Das, S. Babu, F. Visentin, S. Palagi, B. Mazzolai, An earthworm-like modular soft robot for locomotion in multi-terrain environments, *Sci. Rep.* (2023).
- [19] X. Qi, H. Shi, T. Pinto, X. Tan, A novel pneumatic soft snake robot using traveling-wave locomotion in constrained environments, *IEEE Robot. Autom. Lett.* 5 (2) (2020) 1610–1617.
- [20] X. Qi, T. Gao, X. Tan, Bioinspired 3D-printed snakeskins enable effective serpentine locomotion of a soft robotic snake, *Soft Robot.* 10 (3) (2022) 568–579.
- [21] C. Branyan, Y. Menguc, Soft snake robots: Investigating the effects of gait parameters on locomotion in complex terrains, in: 2018 IEEE/RSJ International Conference on Intelligent Robots and Systems, IROS, 2018.
- [22] C. Branyan, R. Hatton, Y. Menguc, Snake-inspired kirigami skin for lateral undulation of a soft snake robot, *IEEE Robot. Autom. Lett.* 5 (2) (2020) 1728–1733.
- [23] J. Rieser, T. Li, J. Tingle, D. Goldman, J. Mendelson III, Functional consequences of convergently evolved microscopic skin features on snake locomotion, *Proc. Natl. Acad. Sci.* (2021).
- [24] C. Zhang, J. Chen, J. Li, Y. Peng, Z. Mao, Large language models for human–robot interaction: A review, *Biomimetic Intell. Robot.* 3 (4) (2023) 100131.
- [25] T. Wang, C. Pierce, V. Kojouharov, B. Chong, K. Diaz, H. Lu, D. Goldman, Mechanical intelligence simplifies control in terrestrial limbless locomotion, *Science Robotics* 8 (85) (2021).
- [26] L. Li, S. Ma, I. Tokuda, Y. Tian, Y. Cao, M. Nokata, Z. Li, Embodying rather than encoding: undulation with binary input, in: 2022 IEEE/RSJ International Conference on Intelligent Robots and Systems, IROS, 2022.
- [27] V. Kojouharov, T. Wang, M. Fernandez, J. Maeng, D. Goldman, Anisotropic body compliance facilitates robotic sidewinding in complex environments, 2023, arXiv(2023).
- [28] Vedant J. Allison, Pseudo-rigid-body dynamic models for design of compliant members, *J. Mech. Des.* 142 (3) (2020).
- [29] Y. Yu, Z. Feng, Q. Xu, A pseudo-rigid-body 2R model of flexural beam in compliant mechanisms, *Mech. Mach. Theory* 55 (2012) 18–33.
- [30] Z. Mao, Y. Peng, C. Hu, R. Ding, Y. Yamada, S. Maeda, Soft computing-based predictive modeling of flexible electrohydrodynamic pumps, *Biomimetic Intell. Robot.* 3 (3) (2023) 110114.
- [31] A. Kakogawa, S. Jeon, S. Ma, Stiffness design of a resonance-based planar snake robot with parallel elastic actuators, *IEEE Robot. Autom. Lett.* 3 (2) (2018) 1284–1291.
- [32] B. Yaqoob, A. Rodella, B. Mazzolai, N. Pugno, Investigating the dynamic influence of passive effects on undulatory locomotion in viscous environment and unleashing the potential of hybrid friction, *Extreme Mech. Lett.* 63 (2023) 102048.
- [33] P. Polygerinos, Z. Wang, J. Overvelde, K. Galloway, R. Wood, K. Bertoldi, C. Walsh, Modeling of soft fiber-reinforced bending actuators, *IEEE Trans. Robot.* 31 (3) (2015) 778–789.
- [34] K. Galloway, P. Polygerinos, C. Walsh, R. Wood, Mechanically programmable bend radius for fiber-reinforced soft actuators, in: 2013 16th International Conference on Advanced Robotics, ICAR 2013, 2013.
- [35] C. Branyan, C. Fleming, J. Remaley, A. Kothari, K. Tumer, R. Hatton, Y. Meng, Soft snake robots: mechanical design and geometric gait implementation, in: 2017 IEEE International Conference on Robotics and Biomimetics, ROBOT, 2017.
- [36] C. Branyan, A. Rafsanjani, K. Bertoldi, R. Hatton, Y. Meng, Curvilinear Kirigami skins let soft bending actuators slither faster, *Front. Robot. AI* 9 (2022).